crystals

MDPI

Communication

Fabrication and Properties for Thermal Neutron Detection of $^{6}LiCl/Rb_2CeCl_5$ Eutectic Scintillator

Rei Sasaki [1,2], Kei Kamada [2,3,4,*], Masao Yoshino [3,4], Kyoung Jin Kim [3,4], Rikito Murakami [2,4], Takahiko Horiai [3,4], Akihiro Yamaji [2,3], Shunsuke Kurosawa [2,3,5], Yuui Yokota [2,3], Hiroki Sato [2,3], Yuji Ohashi [2,3], Takashi Hanada [2] and Akira Yoshikawa [2,3,4]

1 Department of Materials Science, Graduate School of Engineering, Tohoku University, Sendai, Miyagi 980-8579, Japan
2 Institute for Materials Research, Tohoku University, 2-1-1 Katahira Aoba-ku, Sendai, Miyagi 980-8577, Japan
3 New Industry Creation Hatchery Center, Tohoku University, 6-6-10 Aoba, Aramaki, Aoba-ku, Sendai, Miyagi 980-8579, Japan
4 C&A corporation, 1-16-23 Ichibancho, Aoba-ku, Sendai, Miyagi 980-0811, Japan
5 Institute of Laser Engineering, Osaka University, 2-6 Yamadaoka, Suita, Osaka 565-0871, Japan
* Correspondence: kei.kamada.c6@tohoku.ac.jp; Tel.: +81-22-215-2214

Abstract: The ^{3}He gas is commonly used for the detection of thermal neutrons. However, with the depletion of ^{3}He gas, there is a need to develop new solid scintillators for thermal neutron detection. Solid scintillators containing ^{6}Li, which have large neutron capture cross-sections and a large amount of energy released by transmutation reactions, are commonly used as alternative candidates. However, only single-crystal scintillators are currently used, and their ^{6}Li concentration is limited by their chemical composition. In this study, we designed, grew, and evaluated a new eutectic scintillator, $Rb_2CeCl_5/LiCl$, which can improve the ^{6}Li concentration compared with single-crystal scintillators. Rb_2CeCl_5, which was selected as the scintillator phase, has excellent scintillator properties (light yield: 36,000 photons/MeV, decay time: mostly 24 ns, slightly 153 ns), and is less deliquescent than other halide scintillators. The crystal grown using the vertical Bridgman method exhibited a eutectic phase composed of Rb_2CeCl_5 and LiCl. The eutectic crystals exhibited Ce^{3+} 5d-4f emissions, with a peak between 360 and 370 nm. The Rb_2CeCl_5 phase was identified as the luminescent phase via cathodoluminescence mapping, and 16,000 photons/neutron of the light yield and 56.1 ns of the decay time were observed. This study indicates that the $Rb_2CeCl_5/LiCl$ eutectic scintillator is a promising candidate for use in thermal neutron detectors.

Keywords: halide; scintillator; eutectic; vertical Bridgman (VB) method; thermal neutron; ^{6}Li

check for updates

Citation: Sasaki, R.; Kamada, K.; Yoshino, M.; Kim, K.J.; Murakami, R.; Horiai, T.; Yamaji, A.; Kurosawa, S.; Yokota, Y.; Sato, H.; et al. Fabrication and Properties for Thermal Neutron Detection of $^{6}LiCl/Rb_2CeCl_5$ Eutectic Scintillator. *Crystals* **2024**, *14*, 154. https://doi.org/10.3390/cryst14020154

Academic Editor: Thomas M. Klapötke

Received: 27 November 2023
Revised: 25 January 2024
Accepted: 29 January 2024
Published: 31 January 2024

1. Introduction

The demand for thermal neutron detectors is rapidly increasing for various applications, such as stargazing, safety security, neutron capture therapy, resource exploration, time-resolved structural observation, and single-crystal structure analysis. Furthermore, they are used to observe structures inside materials that contain large amounts of light elements, such as Li-ion batteries and plastics [1–3]. In recent years, there has been growing interest in decommissioning nuclear reactors, and the decommissioning of aging nuclear facilities has progressed worldwide, with 19 units decommissioned and 193 units under decommissioning. In addition, the removal of fuel debris from the primary containment vessels (PCV) of the nuclear power plants in Fukushima Daiichi is planned (to start in FY2023), and its scale will gradually expand. Therefore, the demand for thermal neutron detectors will continue to increase in the future.

To date, thermal neutron detectors have been used, starting with ^{3}He gas detectors [4–6] and followed by BF_3 gas detectors [7,8], $Ce:Cs_2LiYCl_6$ [9,10], Tl,Li:NaI(NaIL) [11,12], and $Ce,Eu:LiCaAlF_6$ [13,14] single-crystal scintillator detectors. The current mainstream is

Ce:Cs_2LiYCl_6, a single-crystal scintillator. Its features include a low density of 3.31 g/cm^3 and low sensitivity to gamma rays, high discrimination between gamma and neutron radiation, and a high light yield of 70,000 photons/neutron. However, because it is a single-crystal scintillator, the ^{6}Li concentration is limited by the chemical composition, and there is a weakness in that the ^{6}Li concentration cannot be increased further. Another issue with Ce:Cs_2LiYCl_6 is its long decay time of 6500 ns. ^{6}Li concentration is one of the most important properties in thermal neutron detection. Therefore, our laboratory has focused on eutectic crystals and has developed eutectic scintillators for neutron detection to increase ^{6}Li concentration. Eutectic scintillators are composed of two phases: a ^{6}Li phase that captures thermal neutrons via the following transmutation reaction (Equation (1)) between ^{6}Li and neutrons, and a scintillator phase that emits scintillation light due to α-rays generated by the transmutation reaction [15]. And ^{3}H also contributes to luminescence because of its higher energy and longer path range than α-rays [16].

$$^6\text{Li} + \text{n} \rightarrow \alpha\text{-ray (2.05 MeV)} + {}^3\text{H (2.73 MeV)} \quad (1)$$

The characteristics of eutectic scintillators include the ability to select a scintillator phase with characteristics suited to the application and high concentration of ^{6}Li. Tl:CsI/LiBr [17] and Ce:LaBr/LiBr [18] are examples of eutectic scintillators with satisfactory properties. $CeCl_3$/LiCl/$SrCl_2$ [19] ternary eutectic crystals have been reported recently. In this study, we focused on eutectic scintillators, with Rb_2CeCl_5 as the scintillator phase and LiCl as the neutron-capture phase. The scintillator phase, Rb_2CeCl_5, has excellent scintillator properties (light yield: 36,000 photons/MeV (γ-ray irradiation), decay times: mostly 24 ns, slightly 153 ns (X-ray irradiation), low density: 3.33 g/cm^3, and slight hygroscopic nature [20]. Because a binary phase diagram did not exist for the system designed in this study, crystals were grown at the assumed eutectic point by referring to the binary system of state of K_2CeCl_5-LiCl, which is a similar system [21]. A eutectic structure consisting of the target phase was confirmed, and the scintillator's properties were evaluated.

2. Materials and Methods

2.1. Crystal Growth

$CeCl_3$, RbCl, and 95% ^{6}Li-enriched LiCl powders (99.99% purity) were used as raw materials. First, the raw materials were sealed in a quartz ampoule with an inner diameter of 6.0 mm in a glovebox filled with Ar gas. The weighed composition of Rb_2CeCl_5/^{6}LiCl eutectic was 26.7 mol% RbCl: 13.3 mol% $CeCl_3$: 60.0 mol% ^{6}LiCl. For this eutectic composition, the volume ratio of Rb_2CeCl_5: LiCl was 82.7:17.3, and the density was 2.57 g/cm^3. The quartz ampoule was taken out of the glove box, and raw materials in the quartz ampoule were baked at 180 °C under a vacuum of ~10^{-1} Pa for 3 h to remove moisture and air. The ampoules were sealed using an oxyhydrogen burner. After sealing, the raw material was heated until it melted and then fabricated using the Vertical Bridgman–Stockbarger (VB) method in the apparatus shown in Figure 1, at a pull-down rate of 0.20 mm/min.

2.2. Evaluation of Microstructure and Scintillation Properties

The fabricated samples were cut using a wire saw to obtain wafers in the cross-sectional direction. Subsequently, the thick samples were polished to 1.0 mm in a dry room. The microstructure in the transverse section was observed using backscattered electron image analysis (BEI) with a Hitachi (Tokyo, Japan) S3400N scanning electron microscope (SEM), and powder X-ray diffraction (XRD) was performed using a Bruker (Billerica, MA, USA) D8 Discover diffractometer with a CuKα X-ray source in the 2θ range of 10–90°, with a 40 mA tube current and 40 kV acceleration voltage for phase identification of the microstructure.

Radioluminescence spectra were measured under X-ray excitation in a dry room to determine the emission wavelengths of the grown samples. An Andor Technology (Belfast, UK) iDus420-OE charge-coupled device (CCD) detector and an Andor Technology SR-163 spectrometer were used to collect data. The quantum efficiency (QE) of the measurement device was used to correct the measured data. Furthermore, the cathodoluminescence

(CL) spectra of each crystalline phase were obtained using a JEOL (Tokyo, Japan) JSM-7800F-PRIME field-emission scanning electron microscope (FE-SEM) equipped with a Horiba (Japan) MP-32M CL detector and a Horiba (Japan) Synapse Plus BIUV CCD. To confirm the thermal neutron detection properties, the decay time and light yield were measured in a dry room. The light yield was calculated by comparing the pulse height spectra of the GS20 Li-glass standard with a light output of 4,000 photons/neutron. The grown sample was irradiated using thermal neutrons (^{252}Cf) and gamma rays (^{60}Co) at room temperature, and the signals were obtained using a Hamamatsu Photonics (Japan) R7600U-200 photomultiplier tube (PMT). Shinetsu (Tokyo, Japan) KF-96H-60000CS optical grease was applied to the grown sample to prevent signal attenuation and set in the PMT. The radioisotope, ^{252}Cf, was placed 15 cm from the sample across a moderator, a 10 cm thick polyethylene plate. The obtained data were then corrected for the QE of the detector, as in RL. The same setup used to measure the light yield was also used to measure the decay time, and the signals were digitized using a digital oscilloscope (TD5032B, Tektronix). The decay time was calculated using the average of 128 waveforms as the decay curve.

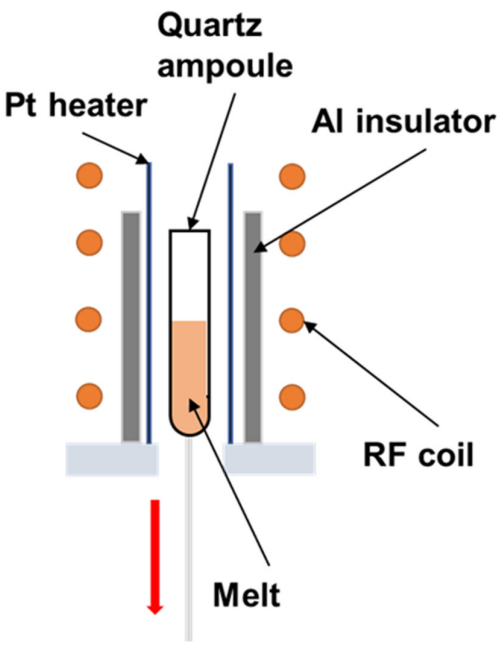

Figure 1. Schematic diagram of crystal growth apparatus.

3. Results

First, microstructural observations of the grown eutectics were carried out. Figure 2 shows a photograph of the growth crystal and 1 mm wafer after cutting and polishing in a dry room. In general, the size requirements for scintillators vary depending on the application. In this study, we aimed to apply the scintillator to thermal neutron beam measurement in the high gamma-ray background environment at the Fukushima Daiichi Nuclear Power Plant. To reduce sensitivity to gamma rays, the scintillator size must be very thin and small (0.1 to 1 mm). Therefore, it is necessary to ensure sufficient transparency at a thickness of 1 mm, and photographs of the crystals were taken at a thickness of 1 mm.

The total length of the crystal grown in the quartz tube was approximately 45 mm. In addition, the photograph of the 1 mm wafer shows that the grown crystal exhibited such transparency that the lines behind it were dimly visible. Figure 3 shows the powder XRD results of the grown eutectics. The broad peaks around 15°~25° originated from the glass cover case to prevent the powder sample from deliquescence during the measurement.

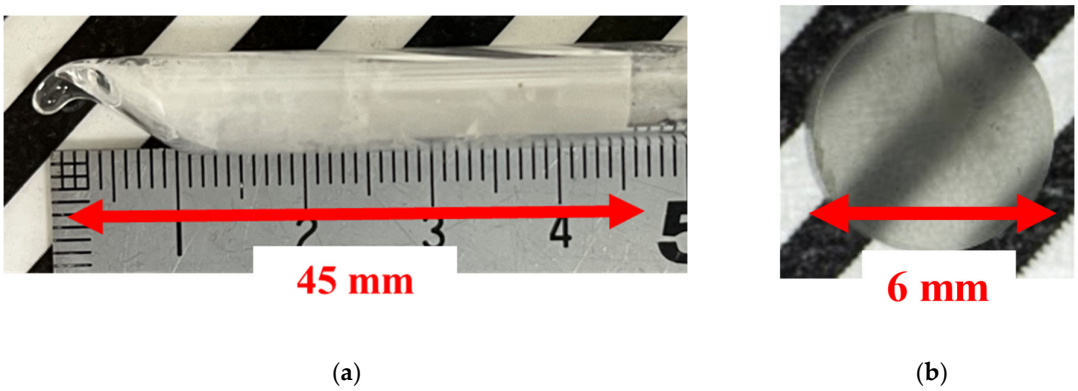

Figure 2. Photograph of as-grown crystal in quartz ampoule (**a**) and 1 mm thick polished wafer (**b**).

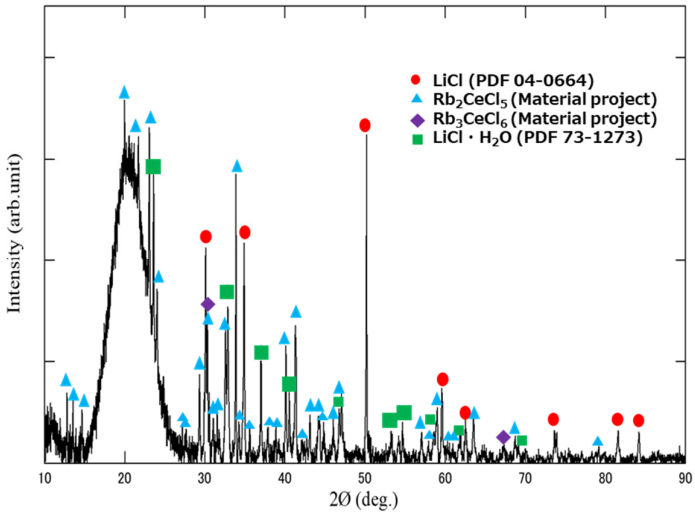

Figure 3. Powder XRD pattern of grown crystal.

Powder XRD results showed a LiCl phase, a LiCl hydrate phase, an Rb_2CeCl_5 phase, and a slight Rb_3CeCl_6 phase; $LiCl{\cdot}H_2O$ was formed by a reaction with the atmosphere when the crystal was powdered, and is not directly related to the grown crystal. Figure 4 shows the result of SEM observation. The grown crystals had a two-phase eutectic structure, and based on the volume ratio, the black matrix areas were considered to be Rb_2CeCl_5, while the white rod areas were LiCl. The molecular weight and contrast were reversed, but this was due to the measurement setup. As in the previous study, the powder XRD results showed a slight Rb_3CeCl_6 phase, but it was too small to be confirmed by means of SEM observations. The powder XRD results and SEM-BEI show that the targeted crystals, Rb_2CeCl_5/LiCl eutectic, were obtained.

Next, the scintillator properties are shown. Figure 5 shows the resulting radioluminescence spectrum measured using X-ray excitation, with a peak between 360 nm and 370 nm.

This is thought to originate from Ce^{3+} 4f-5d transition and is similar to the radioluminescence spectrum of the single crystal [20]. Figure 6 then shows the results of the cathodoluminescence mapping. Cathodoluminescence spectra were obtained by selectively irradiating electron beams while looking at the BEI to identify the emitting phase. Compared with the BEI observed at the same time, the eutectic structure and luminescent/non-luminescent phases were found to correspond to each other. The rod phase of LiCl did not emit light; only the matrix phase of Rb_2CeCl_5 emitted light. Therefore, it was confirmed that the eutectic sample was luminescent due to the Rb_2CeCl_5 phase.

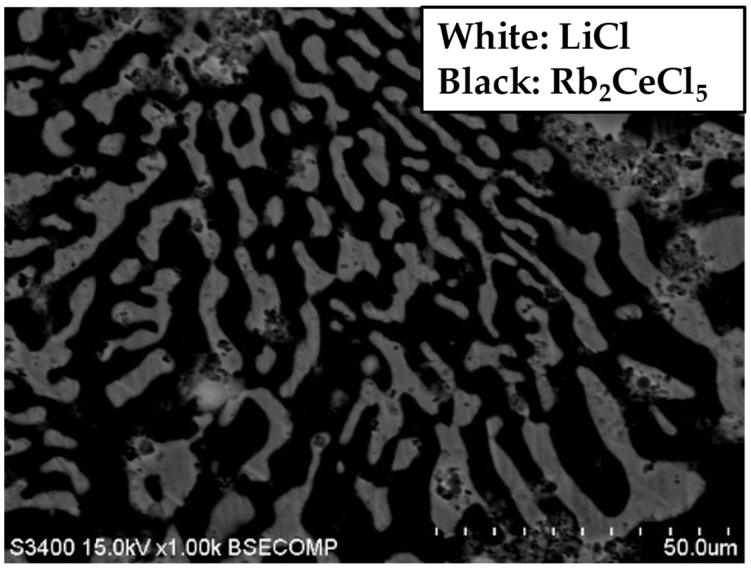

Figure 4. SEM image of the transverse section.

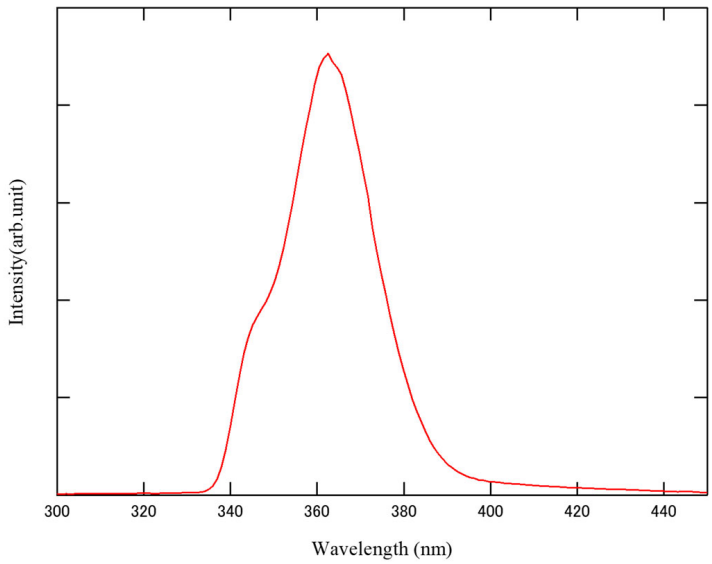

Figure 5. Radioluminescence spectrum of grown crystal under X-ray irradiation.

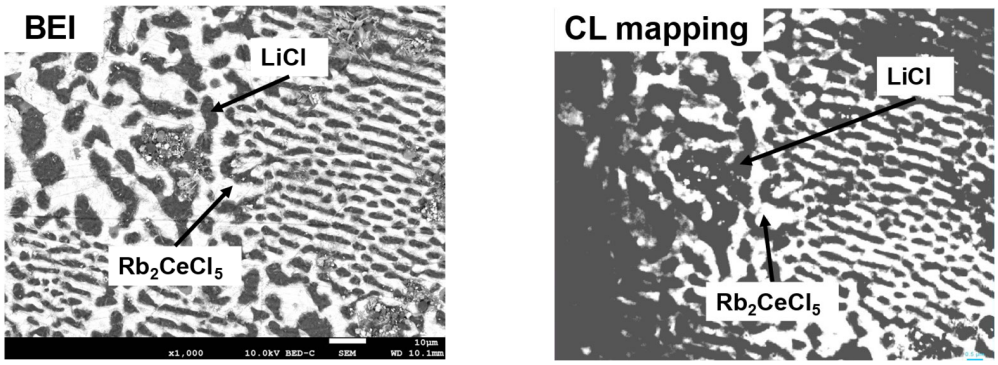

(**a**) (**b**)

Figure 6. SEM-BEI (**a**) and cathodoluminescence mapping of grown crystal (**b**).

Finally, the results of the neutron response are given. Figure 7 shows the luminescence results for the grown crystals and Li-glass; the light yield of the sample was calculated in comparison to the Li-glass standard.

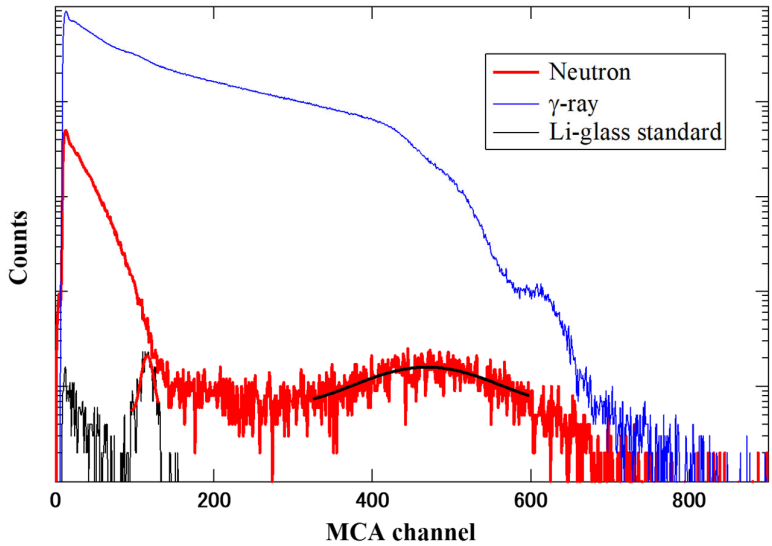

Figure 7. Pulse height spectra of Li-glass standard and fabricated eutectic scintillator.

Below 120, it was considered to be affected by Compton scattering and gamma rays at ^{252}Cf. The pulse height spectra of the eutectics exhibited a broad peak, likely stemming from their growth at a theoretical eutectic point with a relatively moderate growth rate. This condition led to variations in the grain size of the eutectic composition, attenuating certain α-rays before reaching the scintillator phase. However, ^{3}H has a longer path range than α-rays, so the effect of grain size variation is smaller than that of α-rays. The details of the relationship between grain size, energy resolution, and light yield is not clear at this time, but will be clarified in the future through simulations and measurements using samples with different growth rates and composition ratios. Figure 7 illustrates that the peak of the Li-glass standard (4000 photons/neutron, absolute light yield measured) was at 115.8 ± 0.59 Ch., while that of Rb_2CeCl_5/LiCl was at 469.0 ± 3.47 Ch., approximately 400% higher than that of GS20 Li-glass. Taking into consideration both the quantum efficiency (QE) in the photomultiplier tube (PMT) of the Li-glass standard (40%) and the grown crystal (41%), the estimated emission was around 16,000 ± 400 photons/neutron. The emission of gamma-ray excitation is also shown in Figure 7. It was detected as higher on the channel side than at the neutron peak. The light yield was estimated to be 13,600 ± 1000 photons/MeV by comparing the γ-ray peak with that of Tl:NaI (43,000 photons/MeV,QE:39%) [22]. These results show that it is difficult to distinguish neutrons from gamma rays by the difference in light yields in a grown eutectic crystal.

Figure 8 shows the decay curve of the grown crystals. The decay times were estimated to be τ = 56.1 ± 0.4 ns (thermal neutron) and τ = 60.7 ± 0.2 ns (γ-ray) as a result of fitting to the function shown in the figure using the following Equation (2):

$$I = y_0 + A_1 (\exp(-x - x_0)/\tau_1) \quad (2)$$

where each letter in the above equation is I: intensity, y_0: baseline, A_1: constant, x andx: time, and τ_1: decay time. The decay time when irradiated by thermal neutrons was slower than that of the Rb_2CeCl_5 single crystal irradiated by X-ray (24 ns). This phenomenon of different decay times for eutectic crystals and single crystals in the scintillator phase was also observed in previous studies on K_2CeCl_5/LiCl [19]. This may be due to Li^+ substitution into the Rb^+ site of the Rb_2CeCl_5 phase, as in the K_2CeCl_5/LiCl, resulting in a different reaction to neutrons and X-rays, but the detailed mechanism is not known. And

these results show that the grown crystals had difficulty in discriminating neutrons from γ-rays according to the difference in decay times, like the previous study [23–25].

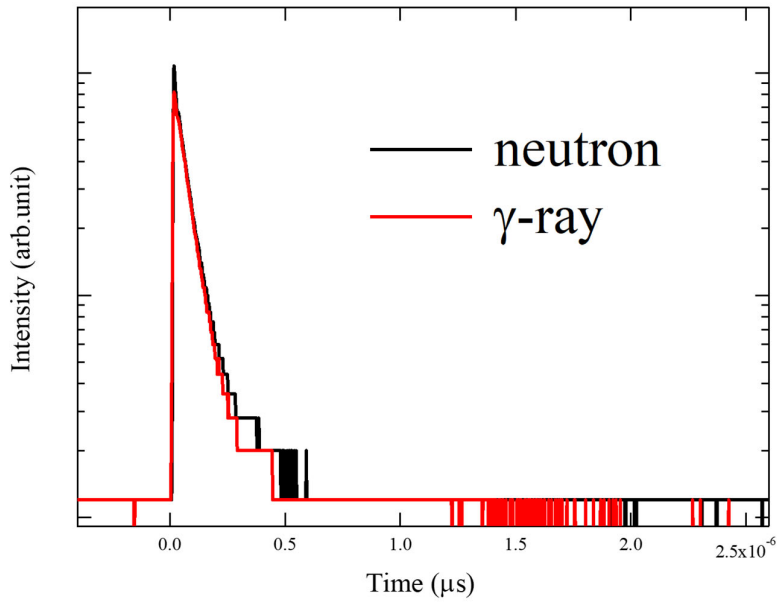

Figure 8. Decay curve and fitting curve of grown crystal.

The actual ^{6}Li concentration could not be calculated in this study because the crystals were grown at a hypothetical eutectic point based on the K_2CeCl_5-LiCl binary system. However, the volume ratio of Rb_2CeCl_5: LiCl = 64:36 and the molar ratio = 20:80 were estimated by analyzing the BEI. From this result, the ^{6}Li concentration was estimated to be 0.039 mol/cm^3.

4. Conclusions

In this study, Rb_2CeCl_5/LiCl was synthesized via the VB method at a theoretical eutectic point, employing a quartz tube with an inner diameter of 6.0 mm. The purpose was to validate the microstructure and assess the scintillator properties. SEM-BEI and powder XRD analyses verified the presence of two phases in Rb_2CeCl_5/LiCl, with a slight Rb_3CeCl_6 phase. The eutectic exhibited a Ce^{3+} 4f-5d emission peak between 360 and 370 nm in the Rb_2CeCl_5 phase, as is consistent with previously reported studies on single crystals of Rb_2CeCl_5. The light yield measured about 16,000 ± 400 photons/neutron, and the single decay component was τ = 56.1 ± 0.2 ns. The density calculated by BEI analysis was notably low at 2.32 g/cm^3, and the eutectic contained 0.039 mol/cm^{-3} of ^{6}Li, surpassing $LiCaAlF_6$ (0.0159 mol/cm^{-3}) and Cs_2LiYCl_6 (0.0052 mol/cm^{-3}) [26].

As the crystals were grown with a hypothesized eutectic composition based on the phase diagram of K_2CeCl_5/LiCl, with a not-so-fast growth rate, there emerged significant variations in the grain size of the eutectic structure. This phenomenon might be responsible for the broadening of the thermal neutron peak in the pulse height spectra and/or the reduction in light yield.

In applications such as fuel debris removal, detecting thermal neutrons amidst a high γ-ray background is crucial. Consequently, scintillators with low density and short decay time are imperative. Additionally, to minimize sensitivity to gamma rays, the scintillator crystals must be exceedingly small (less than 1.0 mm thick). Conversely, they should possess high ^{6}Li content and strong thermal neutron sensitivity. Despite the Rb_2CeCl_5/LiCl eutectic's optical transparency being inferior to single crystals like Cs_2LiYCl_6, it excelled in terms of its higher ^{6}Li content, shorter decay time, and lower density. However, Rb_2CeCl_5/LiCl did not have the expected performance in discriminating neutrons from gamma rays.

In future research, our objective is to enhance scintillator properties by constructing a phase diagram of Rb_2CeCl_5-LiCl and optimizing eutectic fabrication conditions, including

growth rate and temperature. Subsequently, we plan to conduct more comprehensive analyses of thermal neutron response characteristics.

Author Contributions: Conceptualization, R.S. and K.K.; formal analysis, R.S. and M.Y.; funding acquisition, K.K.; investigation, R.S.; methodology, R.S. and K.K.; project administration, K.K.; supervision, A.Y. (Akira Yoshikawa); writing—original draft, R.S. and K.K.; writing—review and editing, R.S., K.K., M.Y., K.J.K., R.M., T.H. (Takahiko Horiai), A.Y. (Akihiro Yamaji), S.K., Y.Y., H.S., Y.O. and T.H. (Takashi Hanada). All authors have read and agreed to the published version of the manuscript.

Funding: This work was partially supported by JSPS KAKENHI, Grant No. 18H01222, 19H00672, 20K20488, 22H04961, 19H00881, 19K12626, and JST CREST, Grant No. JPMJCR2335.

Data Availability Statement: The data presented in this study are available on request from the corresponding author (privacy).

Conflicts of Interest: The authors declare no conflicts of interest. The funders had no role in the design of the study; in the collection, analyses, or interpretation of data; in the writing of the manuscript; or in the decision to publish the results.

References

1. Kardjilov, N.; Manke, I.; Woracek, R.; Hilger, A.; Banhart, J. Advances in Neutron Imaging. *Mater. Today* **2018**, *21*, 652–672. [CrossRef]
2. Butler, L.G.; Schillinger, B.; Ham, K.; Dobbins, T.A.; Liu, P.; Vajo, J.J. Neutron Imaging of a Commercial Li-Ion Battery during Discharge: Application of Monochromatic Imaging and Polychromatic Dynamic Tomography. *Nucl. Instrum. Methods Phys. Res. Sect. A Accel. Spectrometers Detect. Assoc. Equip.* **2011**, *651*, 320–328. [CrossRef]
3. Kardjilov, N.; Manke, I.; Hilger, A.; Strobl, M.; Banhart, J. Neutron Imaging in Materials Science. *Mater. Today* **2011**, *14*, 248–256. [CrossRef]
4. Beddingfield, D.H.; Johnson, N.H.; Menlove, H.O. ^{3}He Neutron Proportional Counter Performance in High Gamma-Ray Dose Environments. *Nucl. Instrum. Methods Phys. Res. Sect. A Accel. Spectrometers Detect. Assoc. Equip.* **2000**, *455*, 670–682. [CrossRef]
5. Kouzes, R.T. *The 3He Supply Problem*; Pacific Northwest National Lab.: Richland, WA, USA, 2009. [CrossRef]
6. Kouzes, R.T.; Ely, J.H.; Erikson, L.E.; Kernan, W.J.; Lintereur, A.T.; Siciliano, E.R.; Stephens, D.L.; Stromswold, D.C.; Van Ginhoven, R.M.; Woodring, M.L. Neutron Detection Alternatives to ^{3}He for National Security Applications. *Nucl. Instrum. Methods Phys. Res. Sect. A Accel. Spectrometers Detect. Assoc. Equip.* **2010**, *623*, 1035–1045. [CrossRef]
7. Rezaei-Ochbelagh, D. Comparison of ^{3}He and BF_3 Neutron Detectors Used to Detect Hydrogenous Material Buried in Soil. *Radiat. Phys. Chem.* **2012**, *81*, 379–382. [CrossRef]
8. Bolewski, A.; Ciechanowski, M.; Dydejczyk, A.; Kreft, A. On the Optimization of the Isotopic Neutron Source Method for Measuring the Thermal Neutron Absorption Cross Section: Advantages and Disadvantages of BF_3 and ^{3}He Counters. *Appl. Radiat. Isot.* **2008**, *66*, 457–462. [CrossRef]
9. Glodo, J.; Hawrami, R.; Shah, K.S. Development of Cs_2LiYCl_6 Scintillator. *J. Cryst. Growth* **2013**, *379*, 73–78. [CrossRef]
10. Lee, D.W.; Stonehill, L.C.; Klimenko, A.; Terry, J.R.; Tornga, S.R. Pulse-Shape Analysis of Cs_2LiYCl_6:Ce Scintillator for Neutron and Gamma-Ray Discrimination. *Nucl. Instrum. Methods Phys. Res. Sect. A Accel. Spectrometers Detect. Assoc. Equip.* **2012**, *664*, 1–5. [CrossRef]
11. Nagarkar, V.V.; Ovechkina, E.; Bhandari, H.; Miller, S.R.; Marton, Z.; Glodo, J.; Soundara-Pandian, L.; Mengesha, W.; Gerling, M.; Brubaker, E. Lithium Alkali Halides-New Thermal Neutron Detectors with n-γ Discrimination. In Proceedings of the 2013 IEEE Nuclear Science Symposium and Medical Imaging Conference (2013 NSS/MIC), Seoul, Republic of Korea, 27 October–2 November 2013; pp. 1–4. [CrossRef]
12. Marshall, M.S.J.; More, M.J.; Bhandari, H.B.; Riedel, R.A.; Waterman, S.; Crespi, J.; Nickerson, P.; Miller, S.; Nagarkar, V.V. Novel Neutron Detector Material: Microcolumnar LixNa1-XI:Eu. *IEEE Trans. Nucl. Sci.* **2017**, *64*, 2878–2882. [CrossRef]
13. Kaburagi, M.; Shimazoe, K.; Terasaka, Y.; Tomita, H.; Yoshihashi, S.; Yamazaki, A.; Uritani, A.; Takahashi, H. Neutron/γ-Ray Discrimination Based on the Property and Thickness Controls of Scintillators Using Li Glass and LiCAF (Ce) in a γ-Ray Field. *Nucl. Instrum. Methods Phys. Res. Sect. A Accel. Spectrometers Detect. Assoc. Equip.* **2023**, *1046*, 167636. [CrossRef]
14. Yokota, Y.; Yamaji, A.; Kurosawa, S.; Ohashi, Y.; Kamada, K.; Yoshikawa, A. Engineering of Eu Dopant Segregation in Colquiriite-Type Fluoride Single Crystal Scintillators. *AIP Adv.* **2017**, *7*, 125312. [CrossRef]
15. Seeger, P.A. Neutron Detection Systems for Small-Angle Scattering. *J. Appl. Crystallogr.* **1988**, *21*, 613–617. [CrossRef]
16. Chuirazzi, W.; Craft, A.; Schillinger, B.; Cool, S.; Tengattini, A. Boron-Based Neutron Scintillator Screens for Neutron Imaging. *J. Imaging* **2020**, *6*, 124. [CrossRef]
17. Yajima, R.; Kamada, K.; Yoshino, M.; Sasaki, R.; Horiai, T.; Murakami, R.; Kim, K.J.; Kochurikhin, V.V.; Ohashi, Y.; Yamaji, A.; et al. Tl Doped CsI/6LiBr Scintillator for Thermal Neutron Detection with Ultra-High Light Yield. *IEEE Trans. Nucl. Sci.* **2023**, *70*, 1331–1336. [CrossRef]

18. Takizawa, Y.; Kamada, K.; Yoshino, M.; Kim, K.J.; Yamaji, A.; Kurosawa, S.; Yokota, Y.; Sato, H.; Toyoda, S.; Ohashi, Y.; et al. Growth and Scintillation Properties of Ce Doped 6LiBr/LaBr3 Eutectic Scintillator for Neutron Detection. *Nucl. Instrum. Methods Phys. Res. Sect. A Accel. Spectrometers Detect. Assoc. Equip.* **2022**, *1028*, 166384. [CrossRef]
19. Yajima, R.; Kamada, K. Fabrication and Characterization of $K_2CeCl_5/^6LiCl$ and $CeCl_3/SrCl_2/^6LiCl$ Eutectics for Thermal Neutron Detection. *Crystals* **2022**, *12*, 1795. [CrossRef]
20. Fujimoto, Y.; Saeki, K.; Nakauchi, D.; Yanagida, T.; Koshimizu, M.; Asai, K. Photoluminescence and Scintillation Properties of Rb2CeCl5 Crystal. *Sensors Mater.* **2019**, *31*, 1241–1248. [CrossRef]
21. He, M.; Lu, G.; Kang, Z.; Zhang, Y. Thermodynamic Assessment of the LiCl-KCl-$CeCl_3$ System. *Calphad Comput. Coupling Phase Diagr. Thermochem.* **2015**, *49*, 1–7. [CrossRef]
22. Holl, I.; Lorenz, E.; Mageras, G. A Measurement of the Light Yield of Common Inorganic Scintillators. *IEEE Trans. Nucl. Sci.* **1988**, *35*, 105–109. [CrossRef]
23. Yang, K.; Menge, P.R.; Ouspenski, V. Enhanced α-γ Discrimination in Co-Doped $LaBr_3$:Ce. In Proceedings of the 2014 IEEE Nuclear Science Symposium and Medical Imaging Conference (NSS/MIC), Seattle, WA, USA, 8–15 November 2014; pp. 1–5. [CrossRef]
24. Vuong, P.Q.; Kim, H.; Luan, N.T.; Kim, S. Neutron Spectroscopy Using Pure $LaCl_3$ Crystal and the Dependence of Pulse Shape Discrimination on Ce-Doped Concentrations. *Nucl. Eng. Technol.* **2021**, *53*, 3784–3789. [CrossRef]
25. Pino, F.; Polo, M.; Delgado, J.C.; Mantovani, G.; Carturan, S.M.; Fabris, D.; Brunelli, D.; Pancheri, L.; Quaranta, A.; Moretto, S. Evidence of Fast Neutron Detection Capability of the CLLB Scintillation Detector. *Radiat. Phys. Chem.* **2023**, *202*, 110494. [CrossRef]
26. Ishikawa, A.; Yamazaki, A.; Watanabe, K.; Yoshihashi, S.; Uritani, A.; Fukuda, K.; Koike, A.; Ogawara, R.; Suda, M.; Hamano, T. Sensitivity and Linearity of Optical Fiber-Based Neutron Detectors Using Small ^{6}Li-Based Scintillators. *Nucl. Instrum. Methods Phys. Res. Sect. A Accel. Spectrometers Detect. Assoc. Equip.* **2020**, *954*, 161661. [CrossRef]